Fifth International Symposium on Marine Propulsors
smp'17, Espoo, Finland, June 2017

Effect of material design parameters on the forced vibration response of composite hydrofoils in air and in water

Andrew W. Phillips[1], Russell Cairns[1], Claire Davis[1], Patrick Norman[1], Paul A. Brandner[2], Bryce W. Pearce[2] and Yin L. Young[3]

[1]Defence Science and Technology Group, 506 Lorimer Street, Port Melbourne VIC 3207, Australia
[2]Australian Maritime College, University of Tasmania, Newnham, TAS 7248, Australia
[3]University of Michigan, Department of Naval Architecture and Marine Engineering, 2600 Draper Dr, 48109 Ann Arbor, MI, USA

ABSTRACT

The ability to tailor the properties of structures made from composite materials gives designers new ways to improve their functionality. For example, the layup of a composite can be designed in such a way that elastic (e.g. bend-twist) couplings advantageously control how the shape and vibration characteristics of the structure changes under load. This ability to tailor composite materials is increasingly being used in marine propeller applications to improve their performance and control their vibration characteristics. However, designers face additional challenges when using these materials. The density of composites approaches that of water so fluid inertial effects become equal to or even greater than solid inertial effects. Moreover, the increased compliance of adaptive composite structures means that they can no longer be considered as approximately rigid, and flow-induced vibrations may develop. This means that load-dependent fluid-structure interaction effects must be understood to enable design optimisation and to avoid unwanted hydroelastic instabilities during operation. In this paper, the forced vibration behaviour of composite hydrofoils designed to have different bending stiffness and bend-twist coupling behaviour were experimentally measured in air and in water tests. Arrays of fibre Bragg gratings (FBG) bonded to the surface of the hydrofoils recorded their dynamic strain response. The effect of added mass on the hydrofoils vibration behaviour is discussed.

Keywords

Fluid-structure interaction (FSI), polymer composite, fibre Bragg grating (FBG), added mass, modal analysis.

1 INTRODUCTION

Historically, marine propellers are designed with the assumption that they are effectively rigid. The rigid assumption greatly reduces the considerable effort required to design marine propellers as the fluid and structural domains can be treated separately. Nevertheless, rigid or fixed geometry designs are approaching their performance limit and new technologies are required to further improve the performance of marine propeller designs. Advanced composites are receiving considerable attention for use in marine propeller blades due to their beneficial properties such as reduced mass, corrosion resistance, anisotropic nature and high fatigue life. These properties can potentially allow marine propellers made from advanced composites to have improved performance characteristics such as increased propulsion efficiency and reduced vibration behaviour as well as lower costs of ownership compared to propellers made from traditional metallic alloys (Young et al. 2016).

Although the potential advantages are evident, designers of composite propellers will need to overcome challenges resulting from their increased flexibility and reduced weight. The reduced mass means that the fluid inertial effects become equal to or even greater than solid inertial effects, while the increased flexibility of adaptive composite structures means the approximately rigid assumption is no longer valid and flow induced vibration may develop. Accordingly, understanding the load dependent fluid-structure interactions (FSI) of light-weight flexible composite structures will be key to preventing any unwanted hydrodynamic instabilities in service.

Good progress has been made in understanding the effect of added mass on the dynamic response of composite structures by coupling structural and fluid numerical models. Lin and Tsai (2008) simulated the effect of added mass on the free vibration characteristics of Magnesium Aluminum Bronze (MAB) and carbon composite propellers. They found that the added mass effect was significantly greater for the composite material than the MAB propeller and demonstrated the significant effect of material anisotropy on both the natural frequency and mode shape. Kramer et al. (2013) and Motley et al. (2013) numerically investigated the dry and wetted vibration characteristics of cantilevered plates made from uniaxial carbon fibre composite. They showed that the added mass effect was influenced by changing the fibre orientation,

particularly for modes greater than the first order. The change in added mass effect was ascribed to an elastic coupling between bending and torsional modes (bend-twist coupling) induced by material anisotropy.

Due to the difficulties in conducting underwater vibration experiments, relatively few experimental works have been performed to understand the effect of added mass on the dynamic response of composite structures. Stenius et al. (2016) experimentally measured the dry and wetted natural frequencies of metal and composite plates in a forced vibration setup. They found that lighter weight and slender structures were affected by the added mass of the water to a greater extent. Kwon et al. (2013) investigated the vibration characteristics of metal, E-glass and carbon composite beams using digital image correlation and found that added mass significantly influenced the mode shapes, particular for the composite beams.

A key challenge with understanding added mass effects is how to measure the dynamic behavior of a structure without affecting its response in-situ in a water environment. Optical fibre sensors have obvious appeal as a candidate for assessing the dynamic response of light weight marine structures. Compared to traditional wired sensors they have a low profile (~125 μm), they have the ability to multiplex sensors along one fibre for distributed sensing, they have excellent immunity to electromagnetic interference and have good compatibility with the marine environment. The most commonly used type of optical strain sensor is the fibre Bragg grating (FBG). An FBG is a localised periodic change in refractive index in the fibre core. FBG strain sensors have recently been successfully used to study the dynamic behavior of a wide range of engineering structures such as wind turbine blades (Kerstin et al. 2006, Lundstrom et al. 2012, Marques dos Santos et al. 2014), helicopter rotor blades (Marques dos Santos et al. 2014), automotive components (Lamberti et al. 2015), composite pipes (Huang et al. 2016) and deep water drilling risers (Liangjie et al. 2014).

In air and in water forced vibration experiments were performed in this study on four composite hydrofoils. The composite hydrofoils were designed and manufactured to have varying bending stiffness and bend-twist coupling behaviours. All hydrofoils had arrays of optical fibre Bragg gratings (FBG) attached to their surface to record their dynamic strain response under the oscillating load. The purpose of the work was to systematically characterise the combined effect of added mass and material design parameters on the vibration behaviour (natural frequencies, mode shapes and damping) of the composite hydrofoils.

2 EXPERIMENTAL

2.1 Manufacture of hydrofoil models

The hydrofoil geometry is shown schematically in Figure 1. The hydrofoil is an unswept trapezoidal planform of 300 mm active span, 120 mm root cord and 60 mm tip cord. The hydrofoil shape was chosen as it contains many of the structural features such as hydrodynamic profile as well as thickness and width tapers found in propeller applications, but without the added geometric complexity that would make manufacture and testing difficult. The hydrodynamic profile was based on a NACA0009 profile but with a thicker trailing edge (see (Zarruk et al. 2014) for more details). The thicker trailing edge allowed for improved manufacturability as well as provided a more robust test piece for subsequent handling, transportation and experimentation.

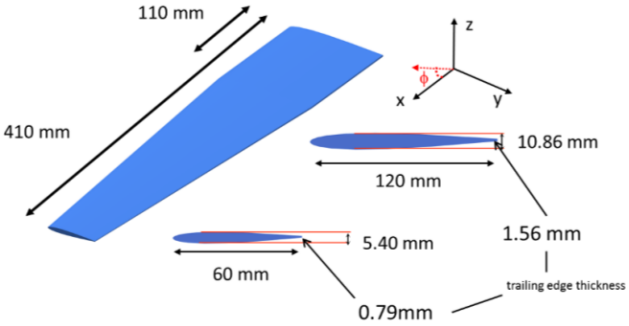

Figure 1. Schematic illustration of the geometric design of the composite hydrofoil.

The hydrofoils were nominally of the same hybrid carbon-epoxy and glass-epoxy construction. Further details of the construction have been published elsewhere (Zarruk et al. 2014, Phillips et al. 2015). The difference between the four hydrofoils was in the orientation of the carbon unidirectional (Carbon-UD) layers. The orientation of the Carbon-UD layers was specifically chosen to allow the influences from bend-twist coupling and flexibility to be separated. In the first hydrofoil, termed GC00, the orientation of the Carbon-UD layers (ϕ) was aligned parallel to the longitudinal axis of the hydrofoil ($\phi = 0^0$). The remaining three hydrofoils had varying Carbon-UD orientations of 15^0 (GC15), 45^0 (GC45) and 90^0 (GC90). In all cases the Carbon-UD fibres were oriented toward the leading edge. All hydrofoils also had a fine 130 g/m^2 basket weave E-glass fabric (Glass-Basket) used as the outer most ply to aid surface quality, protect the structural layers from damage during handling and to prevent any unwanted galvanic effects during testing.

Composite Modeler for ABAQUS was used to help determine the location of the ply drops and accordingly the shape of the individual plies. The templates generated from this process were then used as a guide to cut the dry fabric to the appropriate shape. The hydrofoils were

manufactured using a closed mould resin transfer moulding (RTM) process. A long pot life epoxy (Kinetix R118/H103) was used as the matrix resin. Resin was infused into the part under vacuum. After the part was filled, a pressure of 1 bar (gauge) was applied to aid consolidation until resin gelation. Post cure of the part was performed at 100 °C for a minimum of four hours. After demoulding, any resin flashing remaining on the part was removed using a fine sandpaper and the foils were weighed. Holes were then drilled into the root section to allow assembly in the hydrofoil exciter rig. The density of the hydrofoils can be found in Table 1. The normalised bending stiffness (k_B) and the bend-twist angle (α_{BT}) were also determined using a finite element model with a 1 kN load applied at the approximate centre of pressure of the active span as described previously (Phillips et al. 2015).

Three arrays of nine optical fibre Bragg grating (FBG) sensors were used to measure the surface strains in the active span region of each hydrofoil during testing. The fibre arrays were spanwise oriented along the hydrofoil and as such the nine FBGs per array measured strain in the span direction. The three FBG arrays were mounted parallel to each other and were separated by a distance of 22.5 mm across the chord in the centre of the hydrofoil. The fibres were adhered to the hydrofoil surface using the photo cured optical adhesive NOA061 (Norland). The junction between the sensing fibre and the optical interrogation cable was protected from mechanical stress by a splice protector with a stainless steel insert in the clamped region of the hydrofoil. Figure 2 shows a photograph of an instrumented hydrofoil ready for testing.

Table 1 Summary of the mass properties, normalised bending stiffness (k_B) and bend-twist angle (α_{BT}) of the four hydrofoils.

Hydrofoil	Carbon-UD Orientation (ϕ)	Density (g/cm³)	K_B	α_{BT} (°)
GC00	0	1.56	1.00	0.28
GC15	15	1.51	0.66	-2.40
GC45	45	1.52	0.28	-2.21
GC90	90	1.52	0.23	0.44

Figure 2 Photograph of a hydrofoil instrumented with three arrays of nine optical fibre Bragg gratings (FBGs). The red arrow indicated the orientation of the sensing axis.

2.2 Experimental setup

The hydrofoils were tested both in air and in water in a purpose built water tank at the Australian Maritime College as shown in Figure 3. A hydrofoil exciter rig was bolted to the top of the tank. The exciter rig consisted of a profiled grip assembly which rigidly held the root end of the hydrofoil models. The grip assembly then sat on two linear bearings to allow free moment in the z-axis. A Brüel & Kjær model 4824 electrodynamic shaker excited by a Brüel & Kjær model 2732 power amplifier was used to apply controlled excitations through a sting and the applied force was measured using an in-line Brüel & Kjær model 4824 piezoelectric load cell. For the wet experiments the tank was filled with distilled water up to the top of the active span of the hydrofoil. The free surface at the top of the tank was left open. For the dry experiments the same setup was used except with the water drained from the tank.

In order to generate the strain frequency response functions (SFRFs) for the FBG sensors relative to the input load, the data from different instruments has to be synchronised during acquisition. This was achieved by configuring all instruments to use the same sample clock. The FBG sensors were interrogated using a Micron Optics sm130 running at 2 kHz (the maximum available rate). Each acquisition was started by an external trigger on the "sync in" port and the sample clock for the sm130 was exported on the "sync out" port. Waveform generation and measurement of the input load cell was performed using an NI Compact DAQ 9188 XT chassis with a NI 9263 analog output module and a NI 9215 analog input module. The analog output module was configured to generate arbitrary waveforms such as chirps, slow sine sweeps and random noise bursts. The module output was connected to an amplifier which was used to drive the shaker. Waveforms were generated using the on-board clock at 100 kHz and a trigger denoting the start of the waveform was exported both to the analog input module and an external terminal on the chassis for use by the sm130 and other instruments.

The load cell was connected via a PCB Model 482A16 ICP sensor signal conditioning unit to the NI analog input module. The analog input module was configured to acquire at 2 kHz using the clock exported from the sm130 optical interrogator and to begin each acquisition on the trigger from the analog output module. This configuration meant the data streams from the load cell and FBG sensors would be intrinsically synchronised, greatly simplifying post-processing and enabling real-time generation of FRFs. One disadvantage with this configuration is that constraining the load acquisition to the relatively slow (2 kHz) sample rate of the optical interrogator can result in aliasing if there are any harmonics greater than 1 kHz present in the signal from the load cell.

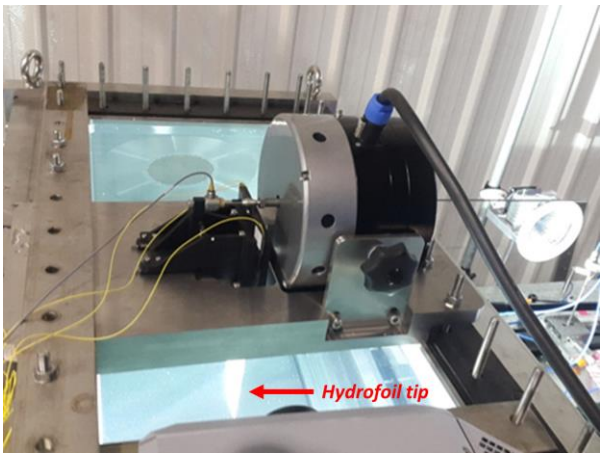

Figure 3 Photo from the top of the tank showing a hydrofoil being tested in the foil exciter rig in the wet condition. The red arrow indicated the location of the hydrofoil tip.

For each test the FBG and load cell data were converted into the frequency domain to the maximum frequency of 1000 Hz and spectral resolution of 0.16 Hz. The SFRF and coherence were then calculated for each FBG sensor using custom designed Python code. The SFRF data was fitted using the poly reference least-squares modal parameter estimator PolyMax™ (Peeters et al. 2004, Peeters et al. 2004) utility within the commercial Siemens LMS Test Lab software. The key advantage of the PolyMax™ utility is that it allows accurate modal parameter estimation in cases where the frequency resolution is low and or the modal density is high. The natural frequencies, mode shapes and damping coefficients of the hydrofoils were determined from the PolyMax™ fitted data.

3 RESULTS & DISCUSSION

3.1 Characterisation of test setup

The quality of modal data from forced vibration experiments is known to be influenced by the excitation profile (Mayes and Gomez 2006). An initial series of tests were performed to determine the most appropriate parameters to use for the excitation profiles applied in these experiments. Burst random and chirp profiles were considered the most appropriate for the experimental program though longer sweep profiles were also investigated. The burst random profile uses a Gaussian distribution of random noise that starts and stops within the time window of one block of data. Burst random profiles will average out non-linear responses and were used in this work to determine the natural frequencies and mode shapes. The burst random profile used 100 averages of 6 s random bursts with a 4 V excitation amplitude.

Chirp profiles use a very fast sine sweep that begins and ends within one time window. Chirp profiles generally have better single to noise characteristics than burst random excitation but do not average out non-linear response. The chirp profile was used in this work to understand the effect of excitation amplitude on the hydrofoils dynamic response, particularly on the damping ratio. Different chirp lengths were investigated between 2 and 120 s. The chirp profile that was deemed to have the best balance between signal quality and experimental time used 100 averages of 6 s sweeps between 10 – 1000 Hz. Excitation voltages ranging from 0.25 – 2 V were examined.

Figure 4 shows plots of both the dry and wetted SFRFs and corresponding coherence for a typical FBG strain sensor near the root of GC45. In both cases, reasonably well defined SFRFs were observed up to limit of the acquisition rate. Although the overall quality was quite good, there were frequency ranges within the SFRFs where the spectral quality was degraded. To further probe the quality of the signal spectrographs, of frequency versus time of the signal were created as shown in Figure 5. The spectrograms indicated that aliasing from higher order modes in the load signal may have affected the SFRF at cross over points. The aliasing effect was worse for the in air experiments. This is probably due to the higher resonance frequencies for in air conditions compared to in water conditions, which make the aliasing effect more severe in the high frequency range. Other reasons could be due to either their reduced response and therefore lower signal to noise compared to the wetted condition, or stronger harmonics above optical fibre interrogation acquisition rate limit. For future experiments, aliasing could potentially be reduced by applying suitable antialiasing filters to the load signal. Nevertheless, the primary interest is in the response of the first five modes, which means frequency less than 800 Hz for dry conditions, and less than 500 Hz for wet conditions. Modes higher than the fifth mode may be influenced by the mass and stiffness of the root support, and hence are not the focus of this work.

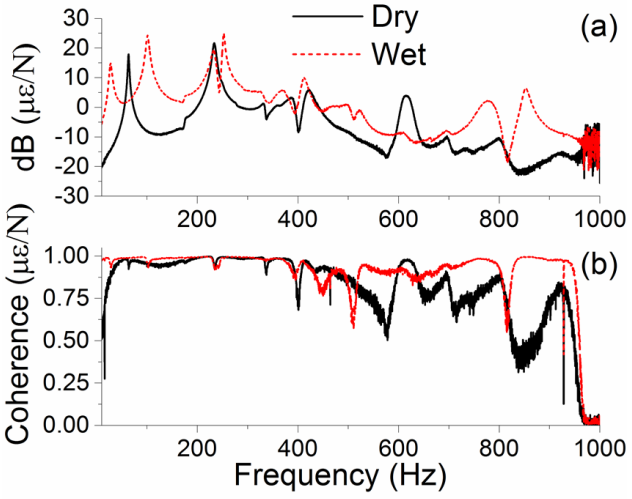

Figure 4 a) Strain Frequency Response Function (SFRF) and b) coherence for strain sensor FBG 1.8 on the GC45 hydrofoil in the dry and wet condition. 4 V 6 s burst random excitation profile.

A possible source of error in these experiments is from extraneous vibrations from the tank windows reflecting back into the water, and thus complicating the measurement of the hydrofoils dynamic behavior. To assess this, the vibrations of the hydrofoil and the tank were simultaneously measured by placing a uniaxial accelerometer on the hydrofoil root and a triaxial accelerometer at various locations on the water tank window. The acceleration data was recorded using a DEWESoft Sirius data acquisition system at a sampling rate of 20 kHz and the signals were converted to the frequency domain. The out-of-plane (z-axis) accelerations of the window were found to be the greatest around the centre of the window, Figure 6. The magnitude of the acceleration at the hydrofoil root was found to be the order of 15x the window vibrations at the first bending mode. The differences between the hydrofoil root and window vibrations were greater still for the higher order modes. The low accelerations of the window compared to the hydrofoil root show that any extraneous excitation resulting from interactions with setup are likely to be low and therefore could reasonably be neglected.

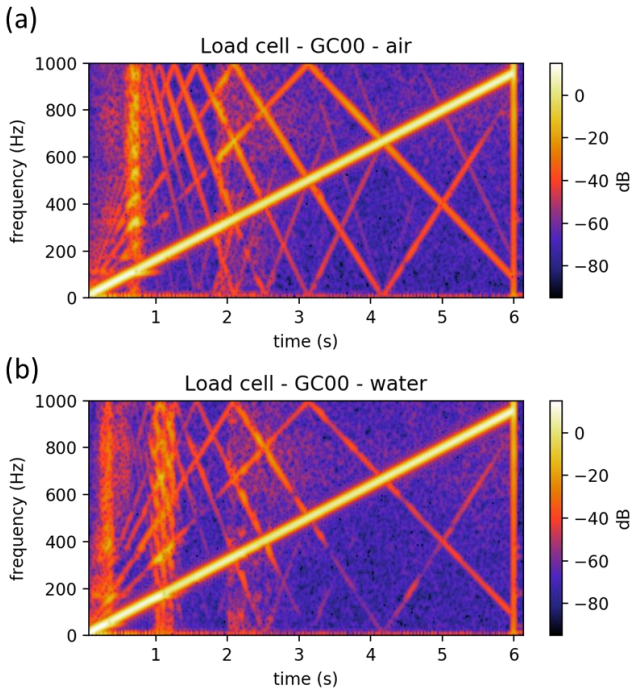

Figure 5 a) in air and (b) in water time versus frequency spectrograms of the response amplitude for the GC00 hydrofoil showing the influence of aliasing from the load signal on the strain frequency response functions. Profile: 6 s chirp 2 V excitation.

3.2 Effect of added mass on natural frequency

Figure 7 shows the effect of Carbon UD angle on the experimentally determined dry and wet natural frequencies for the first five hydrofoil modes. For all hydrofoils and modes investigated, the wetted natural frequency was observed to drop substantially compared to the dry condition. Generally the reduction due to added mass was in the order of 13% to 56% depending on the mode. Changing the Carbon-UD orientation was also shown to have a large influence on both the dry and wetted natural frequencies with the change in natural frequencies being from -28% to +54% depending on the mode. In the dry condition, the modes were reasonably well separated from each other. However, in the wet condition, modes 1 and 2 were close together for GC00 and mode 3 and mode 4 were practically the same value for GC45 and GC90.

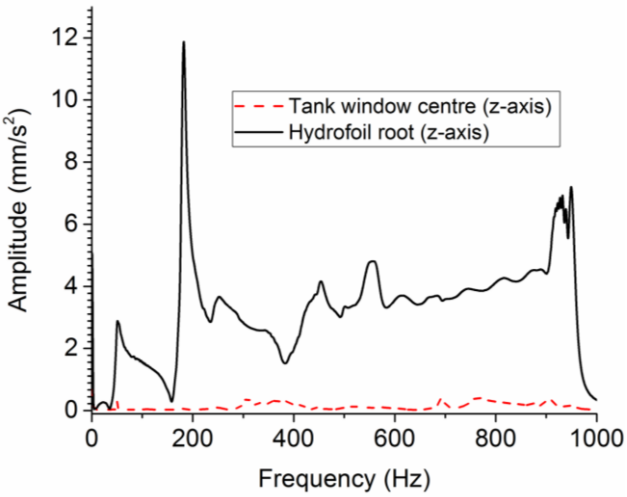

Figure 6 FFT traces showing the relative acceleration of the hydrofoil root and the centre of the water tank window taken during an excitation experiment. Excitation profile: 6 s burst random, 4 V amplitude, wet condition.

To probe the effect of added mass and carbon-UD orientation on the hydrofoils dynamic behaviour a plot of the wet to dry natural frequency ratio ($\omega_{wet}/\omega_{dry}$) was constructed in Figure 7c. Generally the ratios were grouped into two regimes. The first was centred around a ratio of 0.45, while the second was centred around a ratio of 0.65. The different grouping can be explained by a change in mode shape from bending dominated to torsional dominated and are broadly consistent with previous numerical (Kramer et al. 2013) and experimental studies (Kwon et al. 2013) on the effect of added mass on natural frequencies. For comparison, the theoretically predicted effect of added mass for the bending and torsional modes was calculated using theoretical equations based on beam and thin plate theory described by Kramer et al. (2013) and Lindholm et al. (1965).

Pure bending

$$\frac{\omega_{wet}}{\omega_{dry}} = \sqrt{\frac{I_{x,s}}{I_{x,s} + I_{x,a}}} = \left[1 + \frac{3\pi}{32}\frac{\rho_f}{\rho_s}\frac{b}{t}\frac{b^2}{b^2 + t^2}\right]^{-\frac{1}{2}} \quad (1)$$

Pure twisting

$$\frac{\omega_{wet}}{\omega_{dry}} = \sqrt{\frac{m_s}{m_s + m_a}} = \left[1 + \frac{\pi}{4}\frac{\rho_f}{\rho_s}\frac{b}{t}\right]^{-\frac{1}{2}} \quad (2)$$

Where m is the mass; I_x is the mass moments of inertia; ρ is the density; b is the chord; t is the thickness and the subscripts s and f represent solid and fluid respectively. As the bending and torsional modes are primarily out of plane the opposing fluid forces will act in the thickness direction or z-axis. To simplify the hydrofoil geometry for the theoretical analysis the active span was assumed to be a trapezoidal plate with major chord of 120 mm, minor chord of 60 mm, a span of 300 mm and a constant thickness of 10.86 mm. Strip theory as described by Blevins (1979) was then used to approximate the added mass of the trapezoidal plate. The key assumptions in strip theory are that the flow over a thin section or strip of a three-dimensional body is locally two-dimensional and that the interaction between adjacent strips can be neglected.

The results show that Eqs. (1) and (2) provide a good approximation of the lower bound of the wet to dry natural frequency ratio. It should be noted that the equations were derived for thin homogeneous cantilevered plates considering the first bending and first torsional modes only. Hence, some deviation is expected due to the tapered profile of the hydrofoil, and geometric bend-twist coupling effect induced by the forward and aft asymmetry of the modified NACA0009 cross section.

To understand the combined effect of added mass and Carbon-UD orientation in detail the experimentally determined strain mode shapes were determined from the fitted SFRF data. As the strain sensors are aligned along the span of the hydrofoil, the current experimental setup is expected to be the most sensitive to bending modes. The experimental setup is also expected to reveal modes with a torsional component. However, it should be noted that the sensitivity to torsional modes will be somewhat lower as these modes typically generate higher degrees of shear strain than bending modes. Finally, the experimental setup is expected to be relatively insensitive to detecting lead-lag (y-axis) modes. However, in the current experiment lead-lag modes are unlikely to develop to any significant extent as the excitation is primarily out-of-plane (z-axis).

The experimentally determined strain mode shapes were calculated from the SFRFs using the PolyMax^{TM} tool in LMS. Figure 8 shows two dimensional colour map representations of the calculated mode shapes for the GC00 and GC45 hydrofoils. For clarity, the mode shape amplitudes were all normalized to a value of 1. The first mode for both hydrofoils in the wet and the dry condition was predominantly a bending mode. However, even the GC00 hydrofoil showed some torsional component in the first mode. This makes sense as there will be an inherent bend-twist coupled deformation due to the asymmetric forward and aft hydrofoil geometry. The degree of torsional component was higher in GC45 than the GC00 hydrofoil. Again, this is also consistent with the off axis carbon-UD layers resulting in material bend-twist coupling as shown in Table 1.

In GC00 mode 2 and 3 appeared to swap between bending and torsion for the wet and dry condition. Similarly, for GC45 the wetted modes 3 and 4 had higher torsional components compared to the dry condition. It is worthwhile to note that this change in mode shape corresponds to where frequency coalescence was observed in the wetted condition. Combined bending and torsional modes can occur when the centres of bending and twisting as well as the centres of mass and inertia are not co-located. Water loading can shift the effective location of the centers of mass and inertia to different degrees so it is possible for uncoupled modes to become coupled in water. The tapered profile and NACA cross section would exaggerate this effect. The results presented here emphasise the importance of considering the added mass for light weight marine structures, which varies with mode shape, and can be influenced by submergence, speed, cavitation, ventilation, and free surface effects, as noted in (Kramer et al. 2013, Motley et al. 2013, Zarruk et al. 2014, Chae et al. 2016, Harwood et al. 2016, Chae et al. 2017, Young et al. 2017). The variation in added mass can cause unwanted frequency coalescence, as demonstrated in Fig. 7, and in the experimental results shown in Harwood et al. (2016).

3.3 Effect of the surrounding water on damping

Damping is a fundamental quantity that limits vibration amplitudes during service thereby reducing the dynamic loads on the structure. To further probe the influence of the surrounding water on the hydrofoils dynamic behavior, the damping ratio (ζ) was also determined using the PolyMax^{TM} utility. In these experiments, damping may arise from a combination of the material, the structural assembly (friction) and the surrounding fluid (hydrodynamic damping). The damping ratios for the first five dry and wetted modes for the GC00 and GC45 hydrofoils are provided beneath the frequency values under the mode shapes in Figure 8. The effect of the surrounding water on the damping ratio was quite pronounced. Generally, the damping ratios were considerably greater in the wet condition compared to the dry condition. This showed that the total damping in the wetted condition was to a large extent determined by hydrodynamic damping contributions. However, there were a few exceptions to the increased damping in the wetted condition. The first was for mode 2 in GC00 and the second was mode 4 in GC45. In both cases the damping decreased significantly in the wetted condition compared to the dry. This shows that the mode coalescence observed in Figure 7b was associated with a decrease in damping. Nevertheless, it should be noted that the damping values may be influenced by the reflected waves from the tunnel wall boundaries.

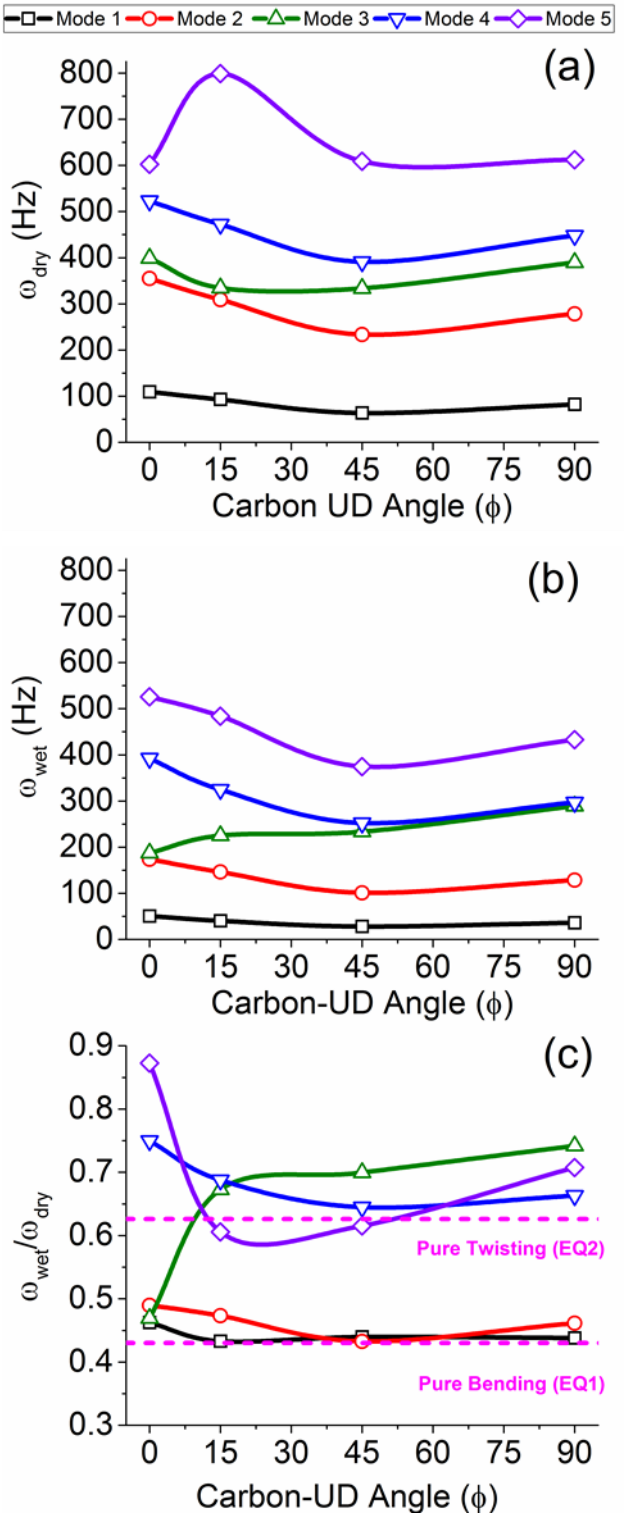

Figure 7 Effect of carbon UD angle (ϕ) on the experimentally determined natural frequencies for the first five modes for (a) dry and (b) wet conditions. (c) The ratio of the wet/dry natural frequencies. Excitation profile: 6 s burst random, 4 V amplitude. The red dotted lines show theoretical calculation of $\omega_{wet}/\omega_{dry}$ ratio for pure bending and torsional modes.

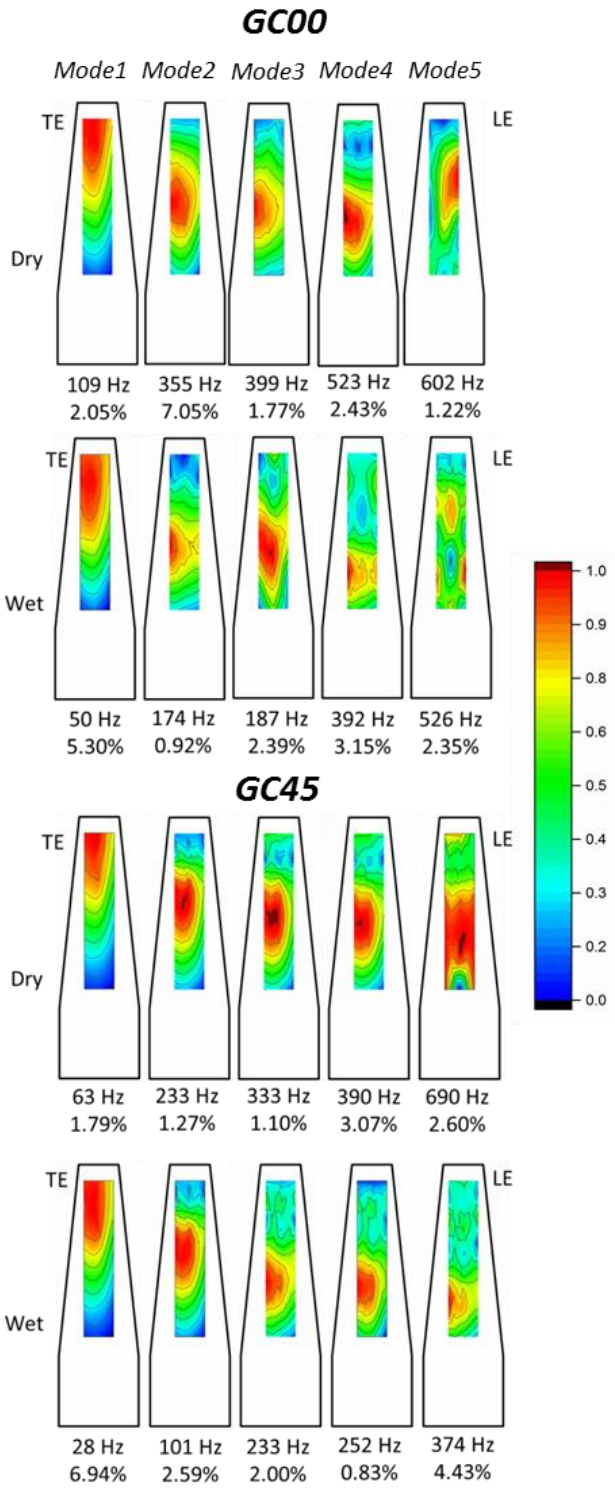

Figure 8 a) experimentally determined strain mode shapes (contours), natural frequencies and damping coefficients for the dry and wet conditions for GC00 and GC45. Colour corresponds to amplitude which has been normalized to a value of 1. Excitation profile: 6 s burst random, 4 V amplitude.

Figure 9 shows the calculated damping ratio for the first hydrofoil mode in air and in water determined using 6 s chirp profiles for three different excitation amplitudes. In the dry condition, the damping ratios were around 1% for all hydrofoils. Previous authors have found a small increase in the damping ratio of cantilevered beams in air with off axis fibre orientations (Mahi et al. 2008). However, the dry damping ratio in the current experiment was found to be relatively insensitive to Carbon-UD orientation.

A possible explanation for the absence of this effect is that any small increase in damping due to the change in Carbon-UD orientation was overwhelmed by damping contribution from the wider structural assembly. The dry damping ratios of the hydrofoils also appeared be insensitive to the excitation amplitude. This is expected as both the material and the structural assembly is expected to be linear under the small deflections that occur in the current experiment.

The damping ratios are much higher in wetted conditions than in dry conditions, where the difference should be due solely to hydrodynamic damping, which includes both radiation and viscous damping. The damping ratio of the first wetted hydrofoil mode was found to increase with increasing Carbon-UD orientation up to a Carbon-UD angle of 45^0. The damping ratio then remained relative constant for a Carbon-UD angle of 90^0. Both GC00 and GC90 hydrofoils did not have any off axis Carbon-UD layers therefore both hydrofoils showed only a small bend-twist response due to the asymmetric nature of the hydrofoil geometry. However, the bending stiffness of the two hydrofoils were considerably different with the GC90 hydrofoil being approximately five times more flexible than GC00. Similarly both GC15 and GC45 hydrofoils had off axis Carbon-UD layers which produced relatively similar bend-twist behavior but different bending stiffness.

Accordingly, the results suggests that the increased damping of the first hydrofoil mode was primarily due to the increased flexibility of the hydrofoils rather than the material anisotropy as shown by the reduction in the hydrofoil bending stiffness values shown in Table 1. The measured wetted damping ratios showed non-linear behavior and were found to increase with increasing excitation amplitude. This further highlights that the hydrodynamic damping is dependent on the vibration amplitude and thus the degree of interaction with the surrounding fluid.

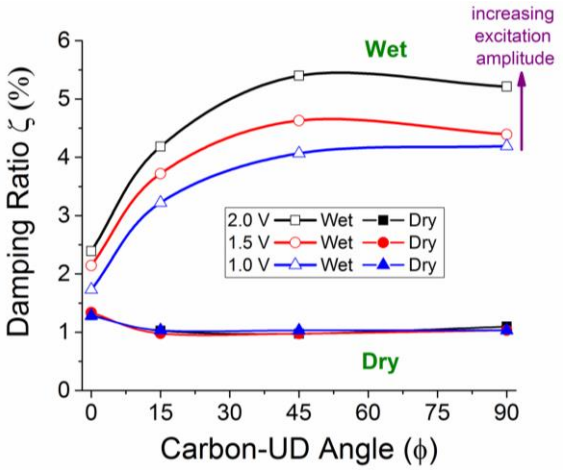

Figure 9 Effect of Carbon-UD angle on the experimentally determined wet and dry damping ratios for mode 1. Profile: 6 s chirp with 1V, 1.5V and 2V excitation amplitude.

4 CONCLUSION

An experimental study was performed which investigated the in air and in water forced vibration behavior of four composite hydrofoils. The hydrofoils were designed and manufactured to have varying bending stiffness and bend-twist coupling behaviours. All hydrofoils had arrays of optical fibre Bragg gratings (FBG) attached to their surface to record their dynamic strain response under an oscillating load. From the results obtained the following was concluded.

1) Spanwise arrays of FBGs attached to the surface of the hydrofoil were successful in capturing at least the first five dry and wetted strain modes for all hydrofoils tested.

2) The natural frequency of the hydrofoils was observed to significantly reduce in water compared to those in air. The added mass effect, as highlighted by the wet to dry natural frequency ratio, was observed to be highly dependent on mode shape with added mass having a greater effect on bending dominated modes compared to torsional dominated modes, which agrees with theoretical calculations.

3) The effect of the surrounding fluids was also observed to have a large influence on damping. The damping of the first bending mode in water was observed to depend on both the orientation of the Carbon-UD layers and the excitation amplitude. However, there was no observed dependence on these parameters for tests performed in air. The results suggest that the hydrodynamic damping component tend to be higher

than the structural damping component, and is highly dependent on the vibration amplitude of the structure in the surrounding fluid.

4) Frequency coalescence was observed for some modes in the wetted condition. The frequency coalescence appeared to be related to a coupling between bending and torsional modes. Furthermore, where frequency coalescence occurred a reduction in the wetted damping ratio was observed.

Finally, the results presented in this paper show that added mass effects can have a considerable influence on the dynamic behavior of light weight and flexible structures. Obtaining a better understanding of the factors which control this will lead to new ways improve propeller designs with enhanced performance characteristics.

5 ACKNOWLEDGMENTS

This project was supported by the Defence Science and Technology Group, the University of Tasmania and the US Office of Naval Research (Dr.Ki-Han Kim, Program Officer) and ONR Global (Dr. Woei- Min Lin) through NICOP S&T Grant N62909-11-1-7013. The authors would like to acknowledge the assistance of Mr Steven Kent and Mr Robert Wrigley from the Australian Maritime College for their essential help with setting up and carrying out the forced vibration experiments.

6 REFERENCES

Blevins, R. D. (1979). Formulas for Natural Frequency and Mode Shape. New York, Van Nostrand Reinhold Company

Chae, E. J., D. A. Akcabay, A. Lelong, J. A. Astolfi and Y. L. Young (2016). "Numerical and experimental investigation of natural flow-induced vibrations of flexible hydrofoils." Physics of Fluids **28**: 075102.

Chae, E. J., D. T. Akcabay and Y. L. Young (2017). "Influence of flow-induced bend–twist coupling on the natural vibration responses of flexible hydrofoils." Journal of Fluids and Structures **69**: 323-340.

Harwood, C., J. Ward, Y. L. Young and S. Ceccio (2016). Experimental Investigation of the Hydro-Elastic Response of a Surface-Piercing Hydrofoil in Multi-Phase Flow. 31st Symposium on Naval Hydrodynamics. Monterey, California**:** 1-19.

Huang, J., Z. Zhou, L. Zhang, J. Chen, C. Ji and D. Pham (2016). "Strain Modal Analysis of Small and Light Pipes Using Distributed Fibre Bragg Grating Sensors." Sensors **16**(10): 1583.

Kerstin, S., E. Wolfgang, A. Jörg, L. Elfrun and L. Gerhard (2006). "A fibre Bragg grating sensor system monitors operational load in a wind turbine rotor blade." Measurement Science and Technology **17**(5): 1167.

Kramer, M. R., Z. Liu and Y. L. Young (2013). "Free vibration of cantilevered composite plates in air and in water." Composite Structures **95**(0): 254-263.

Kwon, Y. W., E. M. Priest and J. H. Gordis (2013). "Investigation of vibrational characteristics of composite beams with fluid–structure interaction." Composite Structures **105**: 269-278.

Lamberti, A., G. Chiesura, G. Luyckx, J. Degrieck, M. Kaufmann and S. Vanlanduit (2015). "Dynamic Strain Measurements on Automotive and Aeronautic Composite Components by Means of Embedded Fiber Bragg Grating Sensors." Sensors (Basel) **15**(10): 27174-27200.

Liangjie, M., L. Qingyou and Z. Shouwei (2014). "Experimental Study of the Vortex-Induced Vibration of Drilling Risers under the Shear Flow with the Same Shear Parameter at the Different Reynolds Numbers." PLoS One **9**(8): e104806.

Lin, H. J. and J. F. Tsai (2008). "Analysis of Underwater Free Vibrations of a Composite Propeller Blade." Journal of Reinforced Plastics and Composites **27**: 447.

Lindholm, U. S., D. D. Kana, W.-H. Chu and H. N. Abramson (1965). "Elastic Vibration Characteristics of Cantilever Plates in Water." Journal of Ship Research **9**: 11-22.

Lundstrom, T., J. Baqersad, C. Niezrecki and P. Avitabile (2012). Using High-Speed Stereophotogrammetry Techniques to Extract Shape Information from Wind Turbine/Rotor Operating Data. Topics in Modal Analysis II, Volume 6: Proceedings of the 30th IMAC, A Conference on Structural Dynamics, 2012. R. Allemang, J. De Clerck, C. Niezrecki and J. R. Blough. New York, NY, Springer New York**:** 269-275.

Mahi, A. E., M. Assarar, Y. Sefrani and J.-M. Berthelot (2008). "Damping analysis of orthotropic composite materials and laminates." Composites Part B: Engineering **39**(7–8): 1069-1076.

Marques dos Santos, F. L., B. Peeters, R. Van der Vorst, W. Desmet and L. C. Sandoval Goes (2014). The use of strain and mixed strain/acceleration measurements for modal analysis. Eurodyn 2014, IX International Conference on Structural Dynamics. Portugal.

Mayes, R. L. and A. J. Gomez (2006). "Part 4: What's shaking', dude? effective use of modal shakers." Experimental Techniques **30**(4): 51-61.

Motley, M. R., M. R. Kramer and Y. L. Young (2013). "Free surface and solid boundary effects on the free vibration of cantilevered composite plates." Composite Structures **96**(0): 365-375.

Peeters, B., G. Lowet, H. Van der Auweraer and J. Leuridan (2004). "A new procedure for modal parameter estimation." Sound and Vibration **38**(1): 24-29.

Peeters, B., H. Van der Auweraer, P. Guillaume and J. Leuridan (2004). The PolyMAX Frequency-Domain Method: A New Standard for Modal Parameter Estimation?**:** 395.

Phillips, A. W., A. Nanayakkara, R. Cairns, N. S. John, M. T. Herath, G. A. Zarruk and P. A. Brandner (2015). Effect of Material Anisotropy on the Structural Response of Flexible Composite Hydrofoils. SAMPE Baltimore 2015. Baltimore**:** #A-9277.

Stenius, I., L. Fagerberg and J. Kuttenkeuler (2016). "Experimental eigenfrequency study of dry and fully wetted rectangular composite and metallic plates by forced vibrations." Ocean Engineering **111**: 95-103.

Young, Y. L., C. M. Harwood, F. Miguel Montero, J. C. Ward and S. L. Ceccio (2017). "Ventilation of Lifting Bodies: Review of the Physics and Discussion of Scaling Effects." Applied Mechanics Reviews **69**(1): 010801-010801-010838.

Young, Y. L., M. R. Motley, R. Barber, E. J. Chae and N. Garg (2016). "Adaptive Composite Marine Propulsors and Turbines: Progress and Challenges." Applied Mechanics Reviews. **062001**: 062001.

Zarruk, G. A., P. A. Brandner, B. W. Pearce and A. W. Phillips (2014). "Experimental study of the steady fluid–structure interaction of flexible hydrofoils." Journal of Fluids and Structures **51**(0): 326-343.